# CALCULATION OF NUCLEAR DATA FOR FAST NEUTRON AND PROTON RADIOTHERAPY: A NEW ICRU REPORT

M.B. Chadwick

University of California, Theoretical Division, Los Alamos National Laboratory, Los Alamos, NM87545

**Abstract**

I discuss the determination of nuclear interaction cross sections that are needed for fast neutron and proton radiotherapy. Both nuclear theory and experimental results are used to evaluate these data. An International Commission on Radiation Units and Measurements (ICRU) report, which is expected to be issued in 1998 and which compiles these data, is described.

# 1 Introduction

A new report describing nuclear data needed in fast neutron and proton radiotherapy studies, which is expected to be issued by the ICRU in 1998, is being written by H.H. Barschall, M.B. Chadwick, P.M. DeLuca, R. Caswell, J.P. Meulders, D.T.L. Jones, H. Schuhmacher, A. Wambersie, and P.G. Young (with L. Cox, J. Siebers, and G.M. Hale acting as consultants). Neutron-induced nuclear reaction cross sections and kerma coefficients are presented in the report up to 100 MeV, and proton-induced cross sections are presented up to 250 MeV. Potential uses of these data include their implementation in radiation transport and treatment planning computer codes to optimize dose delivery to the treatment volume; studies of the impact of nuclear reactions on the relative biological effectiveness of neutron and proton therapy beams; determination of radiation shielding requirements; and use of kerma coefficients to determine absorbed dose for a given neutron distribution, and to convert the absorbed dose, measured with a dosemeter of a given material composition, to absorbed dose in tissue.

The nuclear cross sections are evaluated using a combination of measured data and nuclear model calculations. The ICRU report reviews measurements that have determined cross sections and kerma coefficients (particularly recent works from Davis, Faure, Louvain-la-Neuve, Los Alamos, PTB, Uppsala, and Wisconsin), but since there are only a limited number of experimental data sets for biologically-important target elements, theoretical predictions are needed to supplement these data. The GNASH nuclear model code is used for this purpose, which applies theories for compound nucleus, preequilibrium, and direct reaction mechanisms. Optical model calculations served to determine total, total nonelastic and elastic scattering cross sections. Numerous benchmark comparisons are presented that compare the model predictions with measured data to validate the calculations of energy- and angle-dependent emission spectra, as well as total, nonelastic, and elastic scattering cross sections. For hydrogen, an evaluation is describe that uses both R-matrix and phase-shift scattering theories to represent neutron-proton reaction data. Kerma coefficients are derived from the evaluated neutron-induced cross sections and presented for individual elements as well as ICRU tissue and A-150 plastic.

The current state of knowledge on neutron and proton sources is described in the report, with a particular emphasis on sources at therapy energies. This is important because a calculation of radiation transport and absorbed dose for a therapy beam requires an accurate understanding of the source characteristics. Both thick-target and monoenergetic neutron sources are discussed.

The evaluated cross sections and kerma coefficients are tabulated in the report for neutron- and proton-induced reactions on H, C, N, O, Al, Si, P, Ca, Fe, W, and Pb. Most detailed information is provided for the most important elements, with less information for the others - however, complete tabulations on a fine incident-energy grid is provided for all target elements as electronic files on the accompanying CD. The CD will also contain the same cross section evaluations in the ENDF-6 format which are useful for implementation in radiation transport calculations.

In this paper, I highlight a few results from the forthcoming ICRU report.

# 2 Calculations

The evaluations are based mainly on model calculations using the GNASH code system [1], benchmarked to available experimental data. Some of the major steps involved in this evaluation are: (1) Optical model analyses for $n, p, d, t, \alpha$ particles to generate elastic and nonelastic cross sections, and transmission coefficients; (2) Build a database of low-lying nuclear levels for all product nuclides for use in Hauser-Feshbach and preequilibrium calculations. (3) Match a statistical level density on to the experimental low-lying levels; (4) Use the GNASH code to generate inclusive cross sections based on primary and multiple preequilibrium emission, equilibrium decay, and direct reactions; (5) Use the Kalbach systematics to give continuum angular distributions.

Total, elastic, and nonelastic scattering cross sections are determined using optical model analyses, which are also needed for generating transmission coefficients. Preequilibrium nucleon emission was obtained from the exciton model (and the FKK theory in some cases) and preequilibrium deuteron and alpha cluster emission were obtained from the semiclassical model of Kalbach. Full details of these theories are given in Ref. [2]. We use Hauser-Feshbach theory to calculate equilibrium emission of particles and gamma rays, conserving angular momentum and parity in an open-ended sequence of decay chains. Nuclear level densities were determined using the Ignatyuk model [3], as implemented by Arthur *et al.* [1], which accounts for the washing-out of shell effects with increasing excitation energy.

Our model calculations also include predictions of the yields of nuclides produced in proton-induced reactions, along with their kinetic energy spectra [4]. This is a major development, as high-energy data libraries prior to this work have not included recoil information. Such information is important for calculating the energy deposition in nuclear reactions, since the energy deposited by recoil nuclides can be significant in reactions on light target nuclei. Furthermore, as discussed by Seltzer [5], it can also be used to determine the LET-dependence of ionizing radiation to infer the relative biological effectiveness of neutron and proton therapy beams.

# 3 Results

Neutron-induced data for neutron therapy have been presented (including comparisons with cross section and kerma factor measurements) in Ref. [2]. Therefore a selection of results relevant to proton therapy are presented below.

The evaluated total nonelastic cross sections for protons incident on C and O are shown in Fig. 1, and are seen to describe the experimental data well. Most of the experimental data are compiled in the 1986 review article by Bauhoff [6]. At the lowest energies the nonelastic cross sections decrease, due to the effects of the Coulomb barrier, and eventually drop to zero due to the relatively high excitation energy of the first excited state in these nuclei. An accurate representation of these nonelastic cross sections is particularly important for proton therapy applications since they determine the loss of protons from the proton therapy beam before reaching the treatment volume. Our result for the oxygen total nonelastic cross section is similar to that of Seltzer [5].

Calculated laboratory-frame emission spectra are compared with experimental measurements in Figs. 2–4. These comparisons provide an important benchmarking of the evaluated data libraries and enable their accuracy to be assessed. Based on these comparisons, we have the following conclusions:

- At the lower energies (60 MeV) the calculations proton and alpha emission spectra agree well with the Bertrand and Peelle data [7]. At 90 MeV, the calculations agree well with Fortsch's $^{12}$C$(p,xp)$ data [8].
- At 113 and 256 MeV the calculated $(p,xn)$ spectra are in reasonable agreement with the data [9], but there are some deficiencies: the calculations overpredict the low-energy neutron emission. Additional measurements would be desirable to further understand this discrepancy.

The GNASH code system has been extensively benchmarked for modeling reactions up to 160 MeV. Therefore the present calculations, which extend up to 250 MeV (the upper energy of interest in proton therapy), must be viewed with a certain amount of caution at the highest energies. The comparisons with experimental data here indicate that the calculated cross sections at these higher energies are reasonable, and of comparable quality to LAHET intranuclear cascade results. However, for improved results some further nuclear model developments will be needed in GNASH. Most important is a capability above 150 MeV to include multiple preequilibrium processes for more than two particles. The evaluations will be further tested through comparisons with the new proton-induced emission spectra measurements that will be published by the South African group [10].

# 4 Radiation Transport Calculations

The recent development of data-driven radiation transport codes to determine the absorbed dose and transport of radiation beams in matter has the potential to significantly impact the accuracy of particle therapy treatment-planning.

A new version of the MCNP-LAHET code system is currently being developed at Los Alamos to merge the two code's capabilities into one code, and to make use of new high-energy ENDF data libraries discussed in this paper, and in the paper of Young and Chadwick at this conference. This code system will then be well suited to simulate both the source beam characteristics and the resulting absorbed dose within the patient.

Likewise, at Lawrence Livermore National Laboratory, the PEREGRINE code has the capability to calculate absorbed dose and transport within a patient once the radiation source has been characterized, as discussed in the paper of Cox *et al.* at this conference.

Finally, Medin and Andreo [11] have made use of our proton-induced cross sections on oxygen within their Monte Carlo transport code PETRA, to study stopping powers and the effect of nuclear interactions in proton therapy.

# 5 Acknowledgments

I gratefully acknowledge useful discussions with collaborators in this work: H.H. Barschall, P.M. DeLuca, R. Caswell, J.P. Meulders, D.T.L. Jones, H. Schuhmacher, A. Wambersie, P.G. Young, L. Cox, J. Siebers, G.M. Hale, J. Medin. I am particularly indebted to the late H.H. Barschall for his guidance.

# References

[1] P.G. Young, E.D. Arthur, and M.B. Chadwick, Los Alamos National Laboratory document LA-MS-12343 (1992); M.B. Chadwick and P.G. Young, Phys. Rev. C **47**, 2255 (1993).

[2] M.B. Chadwick, L.J. Cox, P.G. Young, and A.S. Meigooni, Nucl. Sci. Eng. **123**, 17 (1996); M.B. Chadwick and P.G. Young, Nucl. Sci. Eng. **123**, 1 (1996); M.B. Chadwick, P.M. DeLuca, and R.C. Haight, Rad. Prot. Dosim. **70** 1 (1997).

[3] A.V. Ignatyuk, G.N. Smirenkin, and A.S. Tishin, Sov. J. Nucl. Phys. **21**, 255 (1975).

[4] M.B. Chadwick, P.G. Young, R.E. MacFarlane, and A.J. Koning, "High-Energy Nuclear Data Libraries for Accelerator-Driven Technologies: Calculational method for Heavy Recoils", paper at the *2nd. Int. Conf. on Accelerator-Driven Transmutation Technologies and Applications*, 3-7 June 1996, Kalmar, Sweden.

[5] S.M. Seltzer, "An assessment of the role of charged secondaries from nonelastic nuclear interactions by therapy proton beams in water", National Institute of Standards and Technology report NISTIR 5221 (1993).

[6] W. Bauhoff, Atomic Data and Nuclear Data Tables **35**, 429 (1986).

[7] F.E. Bertrand and R.W. Peelle, Phys. Rev. C **8**, 1045 (1973).

[8] K. Lawrie, private communication to MBC (1994); Fortsch *et al.* Nucl. Phys. **A485**, 25 (1988).

[9] M.M. Meier, D.A. Clark, C.A. Goulding, J.B. McClelland, G.L. Morgan, and C.E. Moss, Nucl. Sci. Eng. **102**, 310 (1989); M.M. Meier, C.A. Goulding, G.L. Morgan, and J.L. Ullman, Nucl. Sci. Eng. **104**, 339 (1990).

[10] A. Cowley and W. Richter, private communication to MBC (1997).

[11] J. Medin and P. Andreo, Phys. Med. Biol. **42**, 89 (1997).

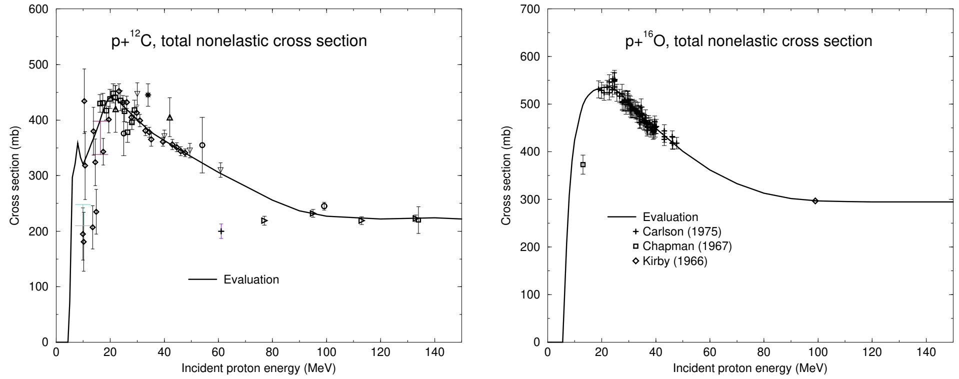


Figure 1: Total nonelastic cross sections compared with experimental data

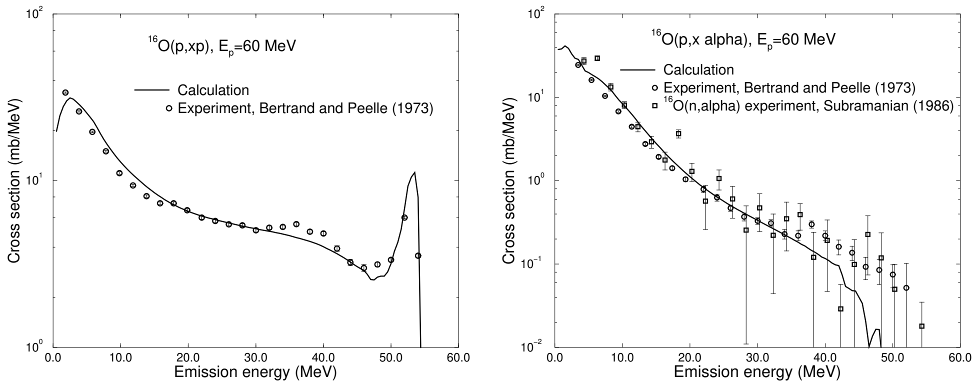


Figure 2: Angle-integrated emission spectra compared with experimental data

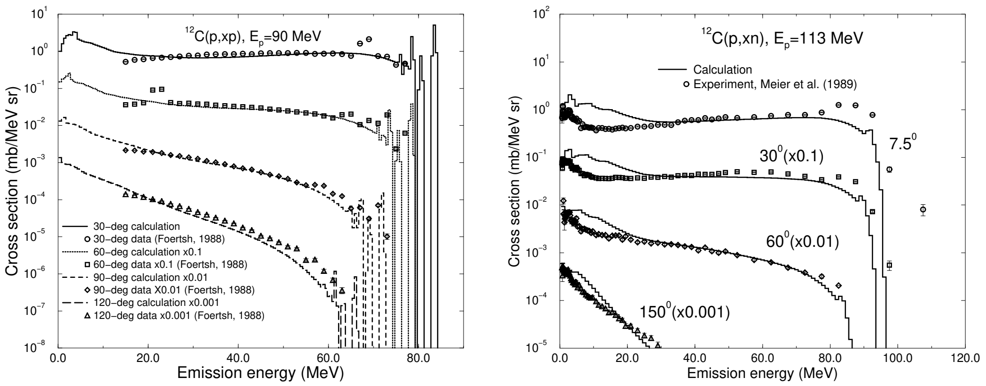


Figure 3: Double-differential emission spectra compared with experimental data

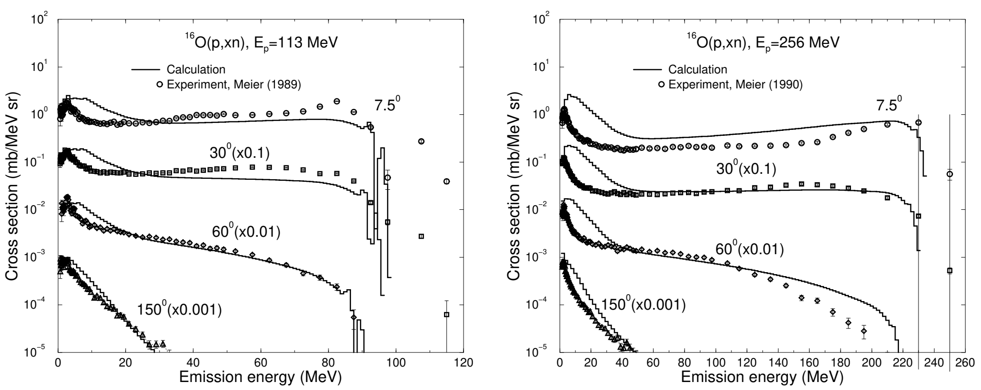


Figure 4: Double-differential emission spectra compared with experimental data